DENT-GLASSER, L. (1979). *Z. Kristallogr.* **149**, 291–325.
DONNAY, G. & ALLMAN, R. (1970). *Am. Mineral.* **55**, 1003–1015.
DUNITZ, J. D. & ORGEL, L. E. (1957). *Nature (London)*, **179**, 462–465.
EWALD, P. P. (1921). *Ann. Phys. (Leipzig)*, **64**, 253–287.
GILLESPIE, R. J. & HARGITTAI, I. (1991). *The VESPR Model of Molecular Geometry*. New York: Prentice Hall.
HAWTHORNE, F. C. (1985). *Am. Mineral.* **70**, 455–473.
HAZEN, R. M. & PREWITT, C. T. (1977). *Am. Mineral.* **62**, 309–315.
HOPPE, R. (1975). *Crystal Structure and Chemical Bonding in Inorganic Chemistry*, edited by C. J. M. ROOYMANS & A. RABENAU, ch. 9, pp. 127–169. Amsterdam: North Holland.
JANSEN, L., CHANDRAN, L. & BLOCK, R. (1991). *J. Mol. Struct.* Submitted.
KHAN, A. A. (1976). *Acta Cryst.* A**32**, 11–16.
KJÄLLMAN, T. & OLOVSSON, I. (1972). *Acta Cryst.* B**28**, 1692–1697.
KRAMER, G. J., FARRAGHER, N. P., VAN BEEST, B. W. H. & VAN SANTEN, R. A. (1991). *Phys. Rev. B*, **43**, 5068–5080.
MAREZIO, M., REMEIKA, J. P. & DERNIER, P. D. (1970). *Acta Cryst.* B**26**, 2008–2022.
MAREZIO, M., SANTORO, A., CAPPONI, J. J., HEWAT, E. A., CAVA, R. J. & BEECH, F. (1990). *Physica C*, **169**, 401–412.
MICHEL, C., HERVIEU, M., BOREL, M. M., GRANDIN, A., DESLENDES, F., PROVOST, J. & RAVEAU, B. (1987). *Z. Phys. B*, **68**, 421–423.
MIEDEMA, A. R., BOOM, R. & DE BOER, F. R. (1975). *Crystal Structure and Chemical Bonding in Inorganic Chemistry*, edited by C. J. M. ROOYMANS & A. RABENAU, ch. 10, pp. 163–196. Amsterdam: North Holland.
MÜLLER-BUSCHBAUM, H. & LEHMANN, U. (1978). *Z. Anorg. Allg. Chem.* **447**, 47–52.
O'KEEFFE, M. (1989). *Struct. Bonding (Berlin)*, **71**, 161–190.
O'KEEFFE, M. (1990). *J. Solid State Chem.* **85**, 108–116.
O'KEEFFE, M. (1991). *Chemistry of Electronic Ceramic Materials*, NIST Special Publication 804, edited by P. K. DAVIES & R. S. ROTH, pp. 485–496. Washington: National Institute of Standards and Technology.
O'KEEFFE, M. & BRESE, N. F. (1991). *J. Am. Chem. Soc.* **113**, 3226–3229.
PANNETIER, J., BASSAS-ALSINA, J., RODRIGUEZ-CARVAJAL, J. & CAIGNAERT, V. (1990). *Nature (London)*, **346**, 343–345.
PAULING, L. (1927). *J. Am. Chem. Soc.* **49**, 765–790.
PAULING, L. (1929). *J. Am. Chem. Soc.* **51**, 1010–1026.
PEARSON, R. G. (1973). Editor. *Hard and Soft Acids and Bases*. Stroudsburg, PA: Dowden, Hutchinson & Ross.
RUTHERFORD, J. S. (1990). *Acta Cryst.* B**46**, 289–292.
RUTHERFORD, J. S. (1991). Private communication.
THOMPSON, J. G., RAE, A. D., WITHERS, R. L. & CRAIG, D. C. (1991). *Acta Cryst.* B**47**, 174–180.
VILLIGER, H. (1969). *DLS Manual*. Institut für Kristallographie und Petrographie, ETH, Zürich, Switzerland.
WAGNER, T. R. & O'KEEFFE, M. (1988). *J. Solid State Chem.* **73**, 211–216.
WALTERSSON, K. (1978). *Acta Cryst.* A**34**, 901–905.
WENK, H. R. & RAYMOND, K. N. (1973). *Z. Kristallogr.* **137**, 86–105.
WU, K. K. & BROWN, I. D. (1973). *Mater. Res. Bull.* **8**, 593–598.
ZACHARIASEN, W. H. (1954). *Acta Cryst.* **7**, 795–799.
ZIOŁKOWSKI, J. & DZIEMBAJ, L. (1985). *J. Solid State Chem.* **57**, 291–299.

Acta Cryst. (1992). B**48**, 572–577

High-Pressure Phases in the System W–O. I. Structure of $WO_{1.09}$ by HRTEM

BY YU. A. BARABANENKOV, N. D. ZAKHAROV AND I. P. ZIBROV

Institute of Crystallography, Academy of Sciences of Russia, Leninsky prospekt 59, Moscow, Russia

V. P. FILONENKO

Institute of High Pressure Physics, Academy of Sciences of Russia, Troitsk, Moscow Region, Russia

AND P. WERNER

Institute of Solid State Physics and Electron Microscopy, Halle/Saale, Germany

(*Received* 25 *March* 1991; *accepted* 15 *November* 1991)

Abstract

A new type of tungsten oxide was synthesized from a mixture of W and WO_3 by a solid-phase sintering method under high-pressure conditions. The crystal structure of the new oxide $WO_{1.09}$ was investigated by selected-area electron diffraction and high-resolution transmission electron microscopy (HRTEM). It has the following unit-cell parameters: $a = 17.16$, $b = 10.32$, $c = 3.78$ Å, $V = 669$ Å^3, $Z = 44$, $\rho = 21$ (3) g cm^{-3}, and belongs to the space group $Cmm2$. The W positions were determined from computer-processed HRTEM structure images. The R-factor minimization procedure was used to refine cationic sites; $R' = 14.5\%$. It is shown that the crystal structure is formed by edge sharing WO_3 octahedrally and tetrahedrally coordinated W cations.

Introduction

High-resolution transmission electron microscopy (HRTEM) provides a unique possibility of investigating the structure of very small crystal fragments of about several hundred ångstroms in size. This size

0108-7681/92/050572-06$06.00

is much smaller than one needs for single-crystal X-ray structure analysis (several hundred micrometres), because electrons are scattered by matter approximately 10^4 times more effectively in comparison with X-rays. As a result, this method is becoming very popular because it allows, in combination with X-ray energy-dispersive microanalysis, investigations of the structure and composition of finely dispersed material (*e.g.* high-temperature superconductors) when there is no possibility of growing large enough single crystals and carrying out X-ray structure analysis. The appearance of a new generation of high-voltage electron microscopes with point-to-point resolution 0.16 nm provides the possibility of localizing the heavy-cation positions in some complex oxides and determining their crystal structure (Zakharov, Gribeluk, Vainshtein, Kovba & Horiuchi, 1988; Zakharov, Gribeluk, Vainshtein, Rozanova, Uchida & Horiuchi, 1983). A new procedure of HRTEM structure analysis has been proposed by Hovmöller, Sjogren, Farrauts, Sundberg & Marinder (1984), which makes it possible to determine cation positions in a complex oxide crystal lattice with an accuracy of about 0.01 nm. The accuracy of this method was corroborated with conventional X-ray structure analysis methods.

The structure and phase composition of WO_x oxides, for x close to 3, have been investigated by many authors (Magnéli, 1949, 1950). But all these investigations were carried out under normal atmospheric pressure and it would be interesting to trace the structure modifications under high-pressure conditions. Up to now the following stable phases in the W–O system, reliably fixed under atmospheric pressure, were known: WO_2, $W_{18}O_{49}$, $W_{20}O_{58}$,WO_3, $W_{12}O_{34}$, W_3O (β-W) (Sundberg, 1978; Magnéli & Andersson, 1955; Palmer & Dickens, 1979; Hartmann, Ebert & Bretschneide, 1931; Roth & Waring, 1966). In the $0 < x < 2$ region only one phase, W_3O, was observed in ultra-fine W powder. The structures of all WO_x oxides (except W_3O) are formed by slightly distorted WO_3 octahedral and pentagonal bipyramids sharing corners or edges. One can reasonably suppose that under high-pressure growth conditions the crystal structure will be more closely packed. As a result, the quota of edge-sharing or even face-sharing octahedra will increase.

The main goal of this work is to investigate the phase composition of WO_x oxides grown under high-pressure conditions and to determine the crystal structure of unknown phases by HRTEM and image-processing methods.

Experimental

The specimens were prepared from W and WO_3 powders mixed in compositions $WO_{0.2n}$, where n = 1–15. Powder mixtures were pressed in the form of pellets 8 mm in diameter and 8 mm high. Subsequently, they were wrapped in Mo foil and placed into a special high-pressure chamber provided with a graphite heater. The pellets were annealed for about 10 min at approximately 6×10^6 kPa and T = 1573 (30) K.

The phase composition of the annealed pellets was investigated by the X-ray powder-diffraction method (Cu $K\alpha$ radiation, Ni filter).

The chemical compositions of the observed new phases were controlled by X-ray energy-dispersive microanalysis (KEVEX system attached to a Hitachi H-500 electron microscope). No other cations except W were detected by this method.

The specimens were examined in a JEOL JEM-4000EX electron microscope equipped with a top-entry high-resolution goniometer and LaB_6 cathode, operated at 400 kV. All the images were obtained under approximately Scherzer defocus conditions ($\Delta f \simeq -48.5$ nm, $C_s = 1$ mm, $\theta_c = 1$ mrad, $E = 400$ kV).

The resolution of the images was measured by optical diffraction methods and was equal to 0.2 nm (2 Å). The region of image characterized by the highest symmetry and corresponding to the thinnest part of the wedge-shaped specimen was digitized in a PDS-1010A microdensitometer using a window size of 10×10 μm and a step size of 10 μm. The latter corresponded to a step of 0.02 nm in the specimen plane. The optical densities, D, all measured in a photo plate, belonged to the interval 0–2 characterized by linear dependence between electron dose and D for the photoemulsion used (ORWO EU-2).

Results

According to the X-ray powder analysis almost all specimens consisted of many different phases except $WO_{2.6}$ which was practically a single phase (the crystal structure of this phase is to be published elsewhere). A second orthorhombic phase, however, was observed in this sample by electron diffraction and HRTEM. The electron microscope image of this phase, used later for image processing, is shown in Fig. 1(*a*). The rectangular region in the experimental image characterized by the highest possible symmetry and corresponding to the thinnest part of wedge-shaped crystal fragment, where the thin-phase object approximation is valid, was selected for digital processing. In the experimental image near the specimen edge, one can usually observe the region where the contrast does not change qualitatively but increases with the specimen thickness. This means that for a given thickness interval, diffracted-beam amplitudes vary almost linearly with the specimen thickness, and the thin-phase object approximation can be used.

Thus, one can visually select the image region in which direct correspondence between image contrast and crystal structure projection is observed.

The two unit-cell parameters a, $b_1 = 0.516$ nm (5.16 Å) and the symmetry elements (two orthogonal symmetry planes *mm*) were determined from the electron microscope image and diffraction pattern taken in the [001] direction (Fig. 1*a*). The third unit-cell parameter c was measured from the image and diffraction pattern taken in the [100] direction (Fig. 1*b*). It should be noted that according to Fig. 1(*b*), the unit cell in the **c** direction incorporates at least two cation layers and the unit-cell parameter b is probably twice as large as the corresponding translation vector $\mathbf{b}_1$ in Fig. 1.

Image processing

The image-processing procedure consisted of several steps:

(i) The rectangular region of the image characterized by the highest symmetry, which corresponded to the thinnest part of the specimen containing an integral number of unit cells, was selected for image processing. It was also important to have a uniform contrast inside this region, because otherwise the additional procedure for background extraction would have to be used.

(ii) The selected image area containing $N \times M$ pixels was linearly transformed into a rectangular region containing $N_1 \times M_1$ pixels, where $N_1 = 2^{\mathrm{Int}(\log_2 N)}$ and $M_1 = 2^{\mathrm{Int}(\log_2 M)}$. This operation makes it possible to arrange an integral number of unit cells in the frame memory of size 256 × 256 pixels and provides the possibility of carrying out the phase refinement procedure for the reflections more accurately.

(iii) The obtained image fragment containing $N_1 \times M_1$ pixels was multiplied by translation in two orthogonal directions to fill the memory having the size 256 × 256 pixels. This operation was followed by the Fourier transformation procedure. Amplitudes and phases of the calculated Fourier components are listed in Table 1. All the calculated reflections were very sharp, and their phases were very well defined, because the processed image fragment contained an integral number of unit cells in both directions.

(iv) From Table 1 it can be seen that the calculated phases of reflections have arbitrary values, because the origin, fully determined by the starting position of the microdensitometer, did not coincide with the position of the twofold axes in the image. The computer program was designed so as to move the position of the origin stepwise in the following way to maximize the function:

$$R(\Delta\mathbf{r}) = \sum_{k=1}^{N} \left| \sum_{j=1}^{M} \mathrm{Re}[f_j \exp(2\pi i \mathbf{g}_j^k \Delta\mathbf{r})] \right|, \qquad (1)$$

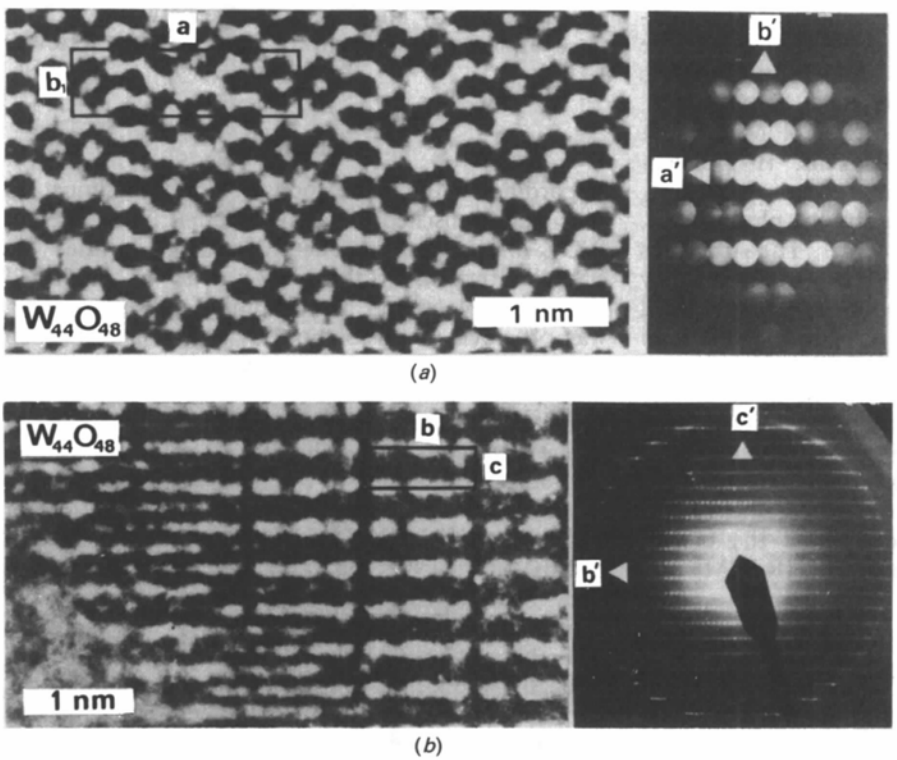

Fig. 1. High-resolution [001] (*a*) and [100] (*b*) micrographs of W oxide and the corresponding electron diffraction patterns. Accelerating voltage of 400 kV with $C_s = 1$ mm and defocus $\Delta f = -50$ nm. Unit-cell parameters $a = 17.16$, $b_1 = 5.16$, $c = 3.78$ Å.

Table 1. *Amplitudes f_i (relative units) and phases φ_i (°) of hkl reflections extracted from the experimental HRTEM image (Fig. 1a)*

$i = 1$, experimental image; $i = 2$ after phase-origin determination; $i = 3$ after symmetrization.

N	h	k	l	f_1	φ_1	f_2	φ_2	f_3	φ_3
1	−2	0	0	0.38	−147	0.38	18	0.38	0
2	2	0	0	0.38	147	0.38	−18	0.38	0
3	−6	0	0	0.43	−121	0.43	16	0.43	0
4	6	0	0	0.43	121	0.43	−16	0.43	0
5	−8	0	0	0.24	−89	0.24	−146	0.24	180
6	8	0	0	0.24	89	0.24	146	0.24	180
7	0	−2	0	0.20	165	0.20	133	0.20	180
8	0	2	0	0.20	−165	0.20	−132	0.20	180
9	1	−1	0	0.54	113	0.54	−167	0.71	180
10	−1	−1	0	0.71	−71	0.71	176	0.71	180
11	−1	1	0	0.54	−113	0.54	167	0.71	180
12	1	1	0	0.71	71	0.71	−176	0.71	180
13	2	2	0	0.78	136	0.78	3	1.00	0
14	−2	2	0	1.00	147	1.00	−15	1.00	0
15	−2	−2	0	0.78	−136	0.78	−3	1.00	0
16	2	−2	0	1.00	−147	1.00	15	1.00	0
17	4	2	0	0.58	137	0.58	−161	0.70	180
18	−4	2	0	0.70	166	0.70	170	0.70	180
19	−4	−2	0	0.59	−137	0.59	161	0.70	180
20	4	−2	0	0.70	−166	0.70	−170	0.70	180
21	−7	−1	0	0.64	174	0.64	−162	0.64	180
22	−7	1	0	0.50	117	0.50	173	0.64	180
23	7	−1	0	0.50	−117	0.50	−173	0.64	180
24	7	1	0	0.64	−174	0.64	162	0.64	180

where j, k summation is carried out over the equivalent reflections, and their groups are correspondingly determined by crystal symmetry; $\Delta\mathbf{r}$ is the image shift, f_j is the amplitude of reflection j and $\mathbf{g}_j^k$ is the corresponding diffraction vector. The phases of all reflections were changed by $\mathbf{g}_j^k\Delta\mathbf{r}'$ after $\Delta\mathbf{r}'$ was found, where $\Delta\mathbf{r}'$ corresponded to the maximum value of $R(\Delta\mathbf{r})$ (see Table 1). Thus, the phases of all reflections are close to 0 or 180°. This means that a new origin coincided with the position of the twofold axis. It should be noted that in (1) the symmetry of the investigated crystal structure is already taken into account. The accuracy of phase-origin determination can be characterized by an average phase deviation α:

$$\alpha = \arctan\sum_j |\mathrm{Im}[f_j \exp(2\pi i \mathbf{g}_j^k \Delta\mathbf{r})]| / \sum_j |\mathrm{Re}[f_j \times \exp(2\pi i \mathbf{g}_j^k \Delta\mathbf{r})]|, \quad (2)$$

which was rather small in our case ($\alpha = 16°$).

(v) The phases of all amplitudes were then assumed to be equal to 0 or 180° depending on which value they were closer to. There were also variations in diffracted amplitudes f_g in each equivalent group observed, owing to small deviations of crystal zone-axis orientation from the electron-beam direction. The maximum f_g value in each equivalent group was chosen because any crystal deviations from the exact zone-axis orientation gave rise to a decrease in f_g. Thereby, the influence of noise and small deviations of crystal orientation from the exact zone axis were eliminated. The resulting image was calculated using a new set of Fourier components (Fig. 2*a*).

(vi) Having analyzed the image contrast distribution and taking into account considerations of crystal chemistry, several structure models were suggested. The theoretical images of these structures were calculated using the weak phase object (WPO) approximation and the microscope phase-contrast function. A rather good correlation between theoretical (Fig. 2*b*) and experimental (Fig. 2*a*) images was observed for one of the proposed structures (Fig. 3). Taking into account the atomic positions as well as image and diffraction pattern symmetry, the space group *Cmm*2 was found to be appropriate.

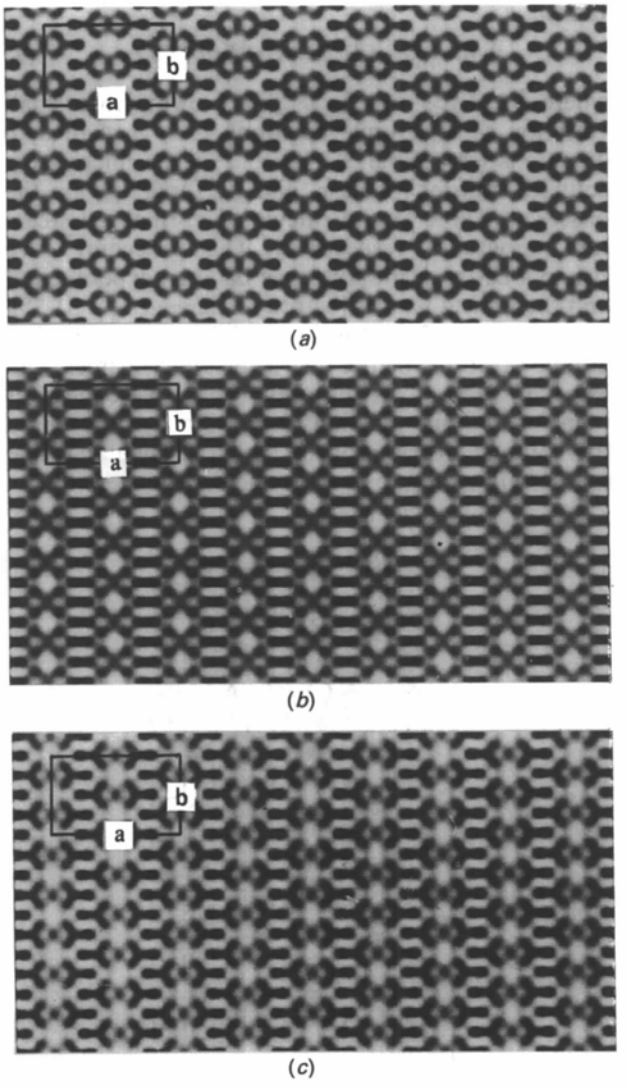

Fig. 2. Numerically processed experimental (*a*) and simulated (*b*), (*c*) electron microscope images of W oxide. (*b*) Image simulated before structure refinement and (*c*) after structure refinement.

(vii) For further structure refinement a method well known in X-ray structure analysis has been used. It implies small variations of cation positions modeled so as to fit intensities of reflections in experimental and theoretical diffraction patterns. This method, however, could not be used for electrons directly, because the intensities of diffracted beams are strongly modified by dynamical scattering effects, and this gives rise to a non-linear dependence of reflection intensities, I_g, on $|f_g|^2$. To refine the structure we compared the moduli of observed structure amplitudes, listed in Table 1, with the calculated ones. In this case the effect of dynamical scattering on I_g was negligibly small, because these amplitudes were obtained from a very thin part of the crystal, where the WPO approximation was valid. The structure refinement was carried out by R-factor minimization:

$$R' = [\sum_{hkl}|F^{obs}_{hkl} - F^{cal}_{hkl}\mathrm{Im}(T)|]/2 \qquad (3)$$

where $\sum_{hkl}|F^{obs}_{hkl}| = 1$, $\sum_{hkl}|F^{cal}_{hkl}| = 1$ owing to a small variation of W atomic positions 1, 2, 3, 4 in **a**, **b** directions (see Table 2), where T is the microscope contrast transfer function, and F^{obs}_{hkl} and F^{cal}_{hkl} are the observed (Table 1) and calculated normalized structure amplitudes, respectively. This procedure gave rise to a better correspondence between experimental and theoretical images [before refinement $R' = 31.7\%$ (Fig. 2*b*) and afterwards $R' = 14.5\%$ (Fig. 2*c*)]. The atomic positions before and after the refinement are listed in Table 2. In the present case we could not refine the atomic positions along the c axis because the contrast distribution in the experimental image was sensitive only to x, y atomic coordinates.

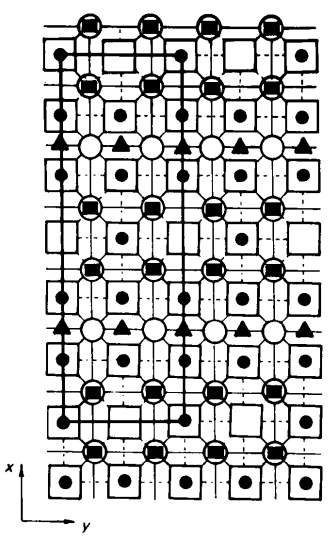

Fig. 3. Idealized structure model of W oxide. Filled symbols: W (● $z = 0$, ■ $z = \frac{1}{2}$, ▲ $z = \frac{1}{4}$); open symbols: O (○ $z = 0$, □ $z = \frac{1}{2}$). Dark lines show the cell with parameters $a = 17.16$, $b_1 = 5.16$ Å.

Table 2. *Atomic coordinates of non-equivalent positions before/after* $WO_{1.09}$ *structure refinement*

Space group *Cmm*2; unit-cell parameters $a = 17.16$, $b_1 = 5.16$, $c = 3.78$ Å.

N		*x*	*y*	*z*
1	W	0.750/0.772	0.000	0.250
2	W	0.868/0.852	0.000	0.000
3	W	0.824/0.805	0.500	0.000
4	W	0.922/0.906	0.262/0.246	0.500
5	W	0.000	0.000	0.000
6	O	0.833	0.000	0.500
7	O	0.000	0.000	0.500
8	O	0.750	0.250	0.000
9	O	0.917	0.250	0.000
10	O	0.833	0.500	0.500
11	O	0.000	0.500	0.500

Concluding remarks

It was shown that the annealing of W–WO_3 samples at about 6×10^6 kPa and 1573 K gives rise to the formation of previously unknown crystal phases. In one of these new phases, whose structure was determined by HRTEM, a network of edge-sharing WO_6 octahedra was observed. It should be noted, however, that besides the WO_6 octahedra, W cations in tetrahedral coordination are incorporated into the crystal structure. Such coexistence of octahedrally and tetrahedrally coordinated W cations was observed earlier in a W–Nb oxide (Roth & Wadsley, 1965). The structure presented here can easily be constructed from metallic W, having a b.c.c. crystal lattice ($a = 3.16$ Å), by adding O atoms at $(00\frac{1}{2})$ and $(\frac{1}{2}\frac{1}{2}0)$ unit-cell positions (Fig. 4). This procedure will give rise to unit-cell distortions (stretching in [001] and shortening in two other directions) and formation of layers of edge-sharing octahedra. In order to obtain the final structure a fraction of octahedrally coordinated cations must be removed and the tetrahedrally coordinated cations must be added (Figs. 3 and 4). The doubling of the unit-cell parameter in the **b** direction can be caused by small displacements of W atoms in alternating directions along the c axis so as to form puckered layers (Hägg, 1935). The density of the proposed crystal structure [$\rho = 21$ (3) g cm^{-3}] appears to be close to the density

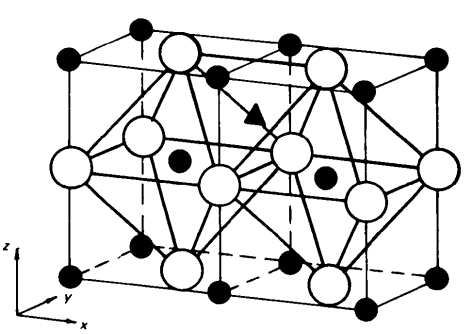

Fig. 4. Construction of the $WO_{1.09}$ structure from metallic W. Filled circles and triangles: W; open circles: O.

of metallic W ($\rho = 19.32$ g cm^{-3}). The HRTEM investigation showed that this structure is rather stable under atmospheric pressure and electron-beam irradiation.

The results of this work demonstrate the high power of HRTEM in structure analysis of very small crystal fragments. Small differences between experimental and theoretical images can be explained by some vagueness of imaging parameters (Δf, C_s, *etc.*).

The procedure of image processing used in this paper is similar to that proposed by Hovmöller, Sjogren, Farrauts, Sundberg & Marinder (1984). However, there are some differences connected with phase-origin determination [equation (1)] and the linear transformation of the selected image area to have integer unit-cell numbers in the frame memory 256 × 256 pixels. We used the structure refinement procedure [equation (3)] and this made it possible to minimize the differences between experimental and theoretical images and to determine the cation positions more accurately. It was found that the effectiveness of this procedure improves as the number of reflections used for image formation increases.

It is a pleasure to thank Drs E. V. Orlova and M. B. Sherman for their skillful assistance and cooperation in image processing.

References

HÄGG, G. Z. (1935). *Z. Phys. Chem. Abt. B*, **29**, 192–196.
HARTMANN, H., EBERT, F. & BRETSCHNEIDE, O. (1931). *Z. Anorg. Chem.* **198**, 127–132.
HOVMÖLLER, S., SJOGREN, A., FARRAUTS, G., SUNDBERG, M. & MARINDER, B.-O. (1984). *Nature (London)*, **311**, 238–241.
MAGNÉLI, A. (1949). *Ark. Kemi*, **1**, 223–227.
MAGNÉLI, A. (1950). *Ark. Kemi*, **1**, 513–518.
MAGNÉLI, A. & ANDERSSON, S. (1955). *Acta Chem. Scand.* **9**, 1378–1381.
PALMER, D. J. & DICKENS, P. G. (1979). *Acta Cryst.* B**35**, 2199–2201.
ROTH, R. S. & WADSLEY, A. D. (1965). *Acta Cryst.* **19**, 26–32, 32–38, 38–42, 42–47.
ROTH, R. S. & WARING, J. L. (1966). *J. Res. Natl Bur. Stand. Sect. A*, **70**, 281–303.
SUNDBERG, M. (1978). *Chem. Scr.* **14**, 161–166.
ZAKHAROV, N. D., GRIBELUK, M. A., VAINSHTEIN, B. K., KOVBA, L. M. & HORIUCHI, S. (1988). *Acta Cryst.* A**44**, 821–827.
ZAKHAROV, N. D., GRIBELUK, M. A., VAINSHTEIN, B. K., ROZANOVA, O. N., UCHIDA, K. & HORIUCHI, S. (1983). *Acta Cryst.* B**39**, 575–579.

Acta Cryst. (1992). B**48**, 577–584

X-ray Standing-Wave Analysis of the Bi Preferential Distribution in $Y_{3-x}Bi_xFe_5O_{12}$ Thin Films

BY A. YU. KAZIMIROV, M. V. KOVALCHUK AND A. N. SOSPHENOV

A. V. Shubnikov Institute of Crystallography of the Academy of Sciences of Russia, Leninsky pr. 59, *Moscow* 117333, *Russia*

V. G. KOHN

I. V. Kurchatov Institute of Atomic Energy, Kurchatov Square 46, *Moscow* 123182, *Russia*

J. KUB, P. NOVÁK AND M. NEVŘIVA

Institute of Physics of the Czechoslovak Academy of Sciences, Cukrovarnicka 10, 16200 *Prague* 6, *Czechoslovakia*

AND J. ČERMÁK

Czech Technical University, Suchbatarova 4, 16607 *Prague* 6, *Czechoslovakia*

(*Received* 28 *January* 1991; *accepted* 10 *February* 1992)

Abstract

The X-ray standing-wave method was used to study the distribution of bismuth ions on the dodecahedral sublattice of a thin yttrium–bismuth iron garnet film. The film was grown epitaxially on a (001)-oriented substrate of gadolinium gallium garnet. Measurement of the fluorescence of Bi^{3+}, Y^{3+}, Fe^{3+} and Gd^{3+} ions was made under conditions such that an X-ray standing wave was formed during diffraction from the layer studied. We have shown experimentally that the dodecahedral sites c_z and c_{xy} are not

0108-7681/92/050577-08$06.00